Journal of the Chinese Institute of Engineers, Vol. 23, No. 3, pp. 275-288 (2000)

BE ANALYSIS OF DYNAMICS OF RIGID FOUNDATIONS EMBEDDED IN TRANSVERSELY ISOTROPIC SOILS

Yaoping Wang and Nimal Rajapakse*
Department of Civil and Geological Engineering
University of Manitoba
Winnipeg, Canada R3T 5V6

Key Words: anisotropy, boundary element method, dynamics, foundations.

ABSTRACT

The dynamic response of rigid massless cylindrical and hemispherical foundations embedded in transversely isotropic elastic soils is investigated in this study. The axis of symmetry of the foundation is assumed to be parallel to the material axis of symmetry of soil. The foundations are subjected to time-harmonic forces acting in the vertical and horizontal directions and a time-harmonic moment. The problems under consideration are solved by using the boundary element method. The kernels of the boundary integral equation correspond to elastodynamic Green's functions of a transversely isotropic elastic half space subjected to buried ring loads. Analytical solutions for Green's functions are used in the analysis. The solutions for impedances obtained from the present study are compared with those reported in literature for foundations embedded in isotropic soils. Selected numerical solutions are presented to portray the influence of material anisotropy, frequency of excitation and foundation geometry on impedances.

I. INTRODUCTION

Analytical solutions for embedded foundations subjected to dynamic loading can be obtained for a few special cases based on linear elasticity. Luco (1976), and Apsel and Luco (1976) presented analytical solutions for torsional response of rigid hemispherical and semi-ellipsoidal foundations embedded in isotropic soils. The majority of existing solutions for dynamics of embedded foundations have been obtained by using approximate analytical or numerical techniques. The Baranov-Novak approach (Baranov, 1967; Novak and Beredugo, 1972) has been used to obtain impedances of rigid cylindrical foundations by uncoupling the soil reaction at the base of the foundation and assuming that the lateral soil reaction can be evaluated independently by simplyfying the stress field in soil. Kuhlemeyer (1969), Wass (1972), Kausel and Roesset (1975) and Day (1977) developed finite element methods to study dynamics of embedded foundations. Dominguez (1978) and Rizzo *et al* (1985) used the boundary integral equation method to study rigid foundations embedded in isotropic soils respectively. Apsel (1979), Luco and Wong (1986) and Apsel and Luco (1987) used an indirect boundary integral equation method to study foundations embedded in layered viscoelastic soils.

Geomaterials (soils, rocks) are rarely isotropic. Transverse isotropy described by five independent material parameters can be used to model the

*Correspondence addressee

anisotropic behavior of soils (Gibson, 1974; Gazetas, 1983). A review of literature indicates that only a few studies considered soil anisotropy in dynamic soil-structure interaction. Freedman and Keer (1972) considered the dynamics of a rigid strip on an orthotropic elastic half plane. Kirkner (1979) examined the dynamic response of a circular surface foundation on a transversely isotropic medium. Gazetas (1981) presented a semi-analytical procedure to study the dynamics of a rigid strip foundation on an orthotropic soil layer. All of the above studies are concerned with surface footings. Wang and Rajapakse (1991) studied rigid strip foundations embedded in orthotropic soils including the through soil coupling between two embedded foundations. An indirect boundary integral equation method was used in the analysis.

The above studies dealing with soil anisotropy do not consider common cases such as large cylindrical foundations (e.g., bridge piers, tower foundations etc.). Solutions for strip foundations have limited applications in practical situations. The assumption of rigid behaviour is acceptable for stocky and massive foundations supporting large structures. However the flexibility is an important consideration in the study of piles.

The objective of the present study is to apply the boundary element method to study the dynamic response of rigid cylindrical and hemispherical foundations embedded in transversely isotropic elastic soils. The foundations are subjected to time-harmonic loading as shown in Fig. 1. The response of the foundation is characterized by vertical, horizontal, rocking and coupled impedances. The convergence and accuracy of the present boundary element solutions are established by comparing with the existing solutions for foundations in isotropic soils. The influence of soil anisotropy, frequency of excitation and foundation geometry on the dynamic response is discussed.

II. GREEN'S FUNCTIONS

Consider a homogeneous transversely isotropic soil with a Cartesian and cylindrical polar coordinate systems defined as shown in Fig. 1. The z-axis is parallel to the material axis of symmetry and normal to the free surface of the soil. The stress-strain relationship for a homogeneous transversely isotropic material can be expressed as (Lekhnitskii, 1963)

$$\sigma_{rr}=c_{11}\epsilon_{rr}+c_{12}\epsilon_{\theta\theta}+c_{13}\epsilon_{zz} \tag{1}$$

$$\sigma_{\theta\theta}=c_{12}\epsilon_{rr}+c_{11}\epsilon_{\theta\theta}+c_{13}\epsilon_{zz} \tag{2}$$

$$\sigma_{zz}=c_{13}\epsilon_{rr}+c_{13}\epsilon_{\theta\theta}+c_{33}\epsilon_{zz} \tag{3}$$

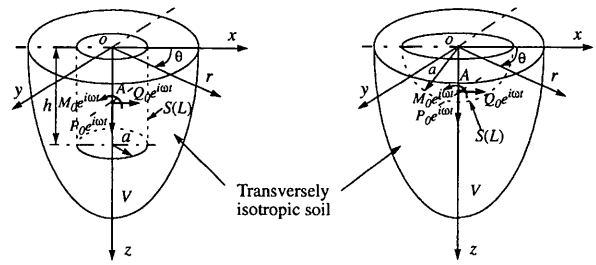

(a) Embedded cylindrical foundation (b) Embedded hemispherical foundation

Fig. 1 Axisymmetric foundations embedded in an elastic soil

$$\sigma_{r\theta}=(c_{11}-c_{12})\epsilon_{r\theta} \tag{4}$$

$$\sigma_{\theta z}=2c_{44}\epsilon_{\theta z},\quad \sigma_{rz}=2c_{44}\epsilon_{rz} \tag{5}$$

where c_{11}, c_{12}, c_{13}, c_{33} and c_{44} denote the material constants of a transversely isotropic soil.

Positive definiteness of strain energy requires that $c_{11}>0$, $c_{33}>0$, $c_{44}>0$, $c_{11}>|c_{12}|$ and $(c_{11}c_{33}-2c_{13}^2+c_{12}c_{33})>0$ (Payton, 1983).

In geotechnical engineering practice, it is common to use a set of Young's moduli (E_h, E_v), a shear modulus (G_{vh}) and three Poisson's ratio (ν_{hh}, ν_{vh}, ν_{hv}) instead of the stiffness coefficients c_{ij} appearing in the Eqns. (1)-(5). The moduli E_h, E_v and G_{vh} denote the Young's moduli in the x (also y) and z directions, and the shear modulus in the plane xz (also yz). The Poisson's ratios ν_{hh}, ν_{hv} denote the transverse contraction in the plane of isotropy to tension on the same plane and tension in the vertical direction respectively. The material constants E_h, E_v, G_{vh}, ν_{hh} and ν_{hv} can be related to the coefficients c_{ij} in the Eqs. (1)-(5) in the following manner.

$$E_h=\frac{(c_{11}-c_{12})(c_{11}c_{33}+c_{12}c_{33}-2c_{13}^2)}{c_{11}c_{33}-c_{13}^2} \tag{6}$$

$$E_v=\frac{c_{11}c_{33}+c_{12}c_{33}-2c_{13}^2}{c_{11}+c_{12}} \tag{7}$$

$$\nu_{hh}=\frac{c_{12}c_{33}-c_{13}^2}{c_{11}c_{33}-c_{13}^2} \tag{8}$$

$$\nu_{hv}=\frac{c_{13}}{c_{11}+c_{12}},\quad G_{vh}=C_{44},\ \nu_{vh}/Eh=\nu_{hv}/E_v \tag{9}$$

The application of boundary element method for semi-infinite soil domains requires Green's functions corresponding to a set of ring loads applied in the interior of the soil. The uniform ring loads required in the analysis of an axisymmetric foundation under vertical loading is shown in Fig. 2(a) and 2(b). The analysis of an axisymmetric foundation subjected to a horizontal force in the x-direction and a moment

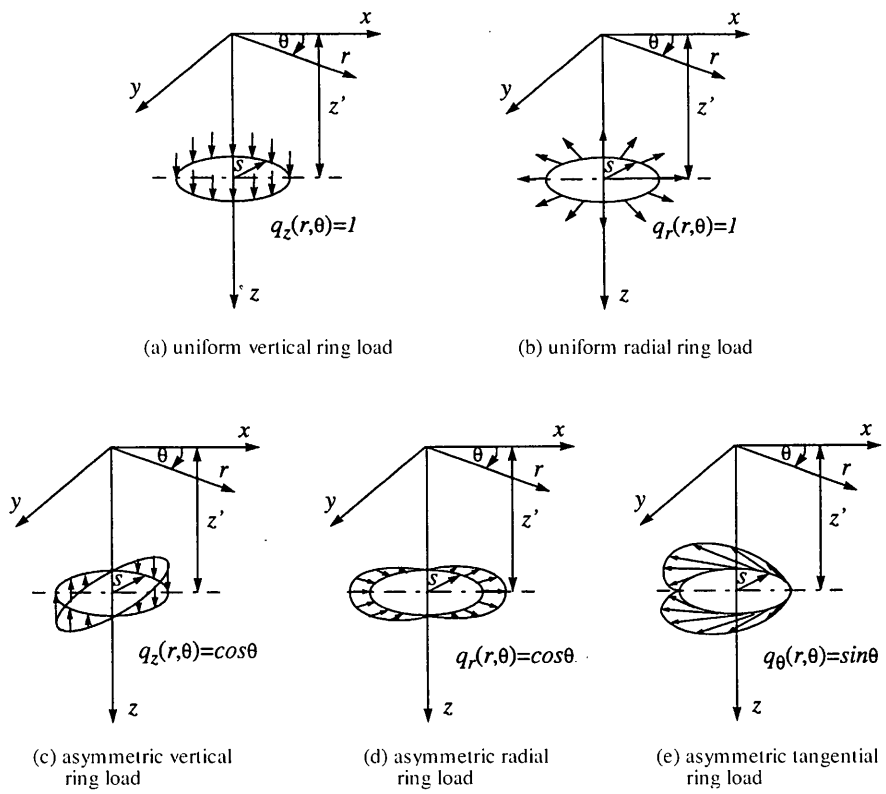

Fig. 2 Buried ring loading required in the boundary element analysis

about the y-direction requires the Green's functions corresponding to three buried ring loads with circumferential variations as shown in Fig. 2(c) to 2(e). Rajapakse and Wang (1993) discussed the derivation of time-harmonic Green's functions for loads applied in the interior of a transversely isotropic elastic half space. The displacement Green's functions corresponding to the loading shown in Fig. 2 are given in the Appendix.

III. DYNAMICS OF RIGID AXISYMMETRIC FOUNDATIONS

Rigid cylindrical and hemispherical foundations subjected to time-harmonic dynamic loads are shown in Fig. 1. The axis of symmetry of the foundation coincides with the z-axis. The foundations are subjected to forces $P_0e^{i\omega t}$ in the z-direction and $Q_0e^{i\omega t}$ in the x-direction and a time-harmonic moment $M_0e^{i\omega t}$ about the y-axis at the point A with coordinates $(0, 0, \overline{z})$. The foundations are assumed to be perfectly bonded to the surrounding soil along the contact surface S. For axisymmetric foundations, the contact surface S can be generated using a curve L in the rz-plane. The displacement at an arbitrary point on the foundation can be expressed in terms of the displacements and rotations of the point A. In the case of a vertically loaded foundation, the displacements at an arbitrary point on S can be expressed as

$$u_r(r, \theta, z)=u_\theta(r, \theta, z)=0 \tag{10}$$

$$u_z(r, \theta, z)=\Delta_V \tag{11}$$

where Δ_V denotes the vertical displacement at the point A.

In the case of a laterally loaded foundation (horizontal and moment loading), the displacements at an arbitrary point on S can be expressed as

$$u_r(r, \theta, z)=[\Delta_H+(z-\overline{z})\phi_y]\cos\theta \tag{12}$$

$$u_\theta(r, \theta, z)=-[\Delta_H+(z-\overline{z})\phi_y]\sin\theta \tag{13}$$

$$u_z(r, \theta, z)=-r\phi_y\cos\theta \tag{14}$$

where Δ_H and ϕ_y denote the horizontal (x-direction) displacement and the rotation about the y-axis of the point A, respectively.

The resultant forces and moment acting on a massless foundation with respect to the point A can be expressed in terms of traction components $T_i(r, \theta, z)$ $(i=x, y, z)$ on S as

$$P_0 = \int_S T_z dS \tag{15}$$

$$Q_0 = \int_S T_x dS \tag{16}$$

$$M_0 = \int_S T_z r\cos\theta dS + \int_S T_x (z - \overline{z}) dS \tag{17}$$

The dynamic response of a rigid foundation under the loading shown in Fig. 1 is characterized by the following nondimensional impedance matrix.

$$\begin{pmatrix} P_0 \\ Q_0 \\ M_0 \end{pmatrix} = ac_{44} \begin{pmatrix} K_V & 0 & 0 \\ 0 & K_H & K_{HM} \\ 0 & K_{MH} & K_M \end{pmatrix} \begin{pmatrix} \Delta_V \\ \Delta_H \\ a\phi_y \end{pmatrix} \tag{18}$$

where K_V, K_H, $K_{MH}(=K_{HM})$ and K_M are the vertical, horizontal, coupled and rocking impedances respectively; 'a' denotes a unit length parameter such as the radius of a cylindrical or hemispherical foundation.

The impedances of a foundation as defined by Eq. (18) can be computed by expressing the tractions in Eqs. (15)-(17) in terms of the rigid body displacements Δ_V, Δ_H and ϕ_y. Such a relationship can be developed through the application of the boundary element method to the soil domain under the vertical and lateral loading cases separately.

Computation of Contact Tractions by BEM

In the case of axially symmetric bodies subjected to asymmetric loading, it is convenient to apply Fourier expansion with respect to θ and reduce a given boundary-value problem to a set of uncoupled problems corresponding to each Fourier harmonic. For a vertically loaded axisymmetric foundation, only the zero-order (m=0) symmetric Fourier harmonic needs to be considered in the modelling of surrounding soil domain. For the loading shown in Fig. 1(b), only the first-order symmetric (m=1) harmonic needs to be considered. The application of direct boundary element method to axially symmetric bodies subjected to asymmetric loading results in the following integral equation for each Fourier harmonic.

$$c_{ij}(\boldsymbol{x}) u_j^m(\boldsymbol{x}) + \int_L H_{ij}^m(\overline{\boldsymbol{x}}, \boldsymbol{x}) u_j^m(\overline{\boldsymbol{x}}) \overline{r}\, dL = \int_L G_{ij}^m(\overline{\boldsymbol{x}}, \boldsymbol{x}) T_j^m(\overline{\boldsymbol{x}}) \overline{r}\, dL \tag{19}$$

where m denotes a Fourier harmonic; (i, j=r, θ, z) and summation is implied over j; $\boldsymbol{x}$ and $\overline{\boldsymbol{x}}$ denote position vectors on the generating curve L; $\overline{r}$ denote the radial coordinate of the point $\overline{\boldsymbol{x}}$; $G_{ij}^m(\overline{\boldsymbol{x}}, \boldsymbol{x})$ and $H_{ij}^m(\overline{\boldsymbol{x}}, \boldsymbol{x})$ are the mth harmonics of displacement and traction Green's functions corresponding to the point $\overline{\boldsymbol{x}}$ in a transversely isotropic half space due to a ring load through a point $\boldsymbol{x}$ having circumferential dependence identical to the mth Fourier harmonic (Fig. 2); $u_j^m(\overline{\boldsymbol{x}})$ and $T_j^m(\overline{\boldsymbol{x}})$ denote the mth harmonic of displacements and tractions at the point $\overline{\boldsymbol{x}}$ on L.

The coefficients $c_{ij}(\boldsymbol{x})$ are given by

$$c_{ij}(\boldsymbol{x}) = \begin{cases} 1, & \boldsymbol{x} \text{ inside } V \\ 1/2, & \boldsymbol{x} \text{ on } L \\ 0 & \boldsymbol{x} \text{ outside } V \end{cases} \tag{20}$$

In the present case, $\boldsymbol{x}$ is selected such that $\boldsymbol{x} \in L$, *ie.*, $\boldsymbol{x}$ is located on the generating curve L, and c_{ij} is equal to 1/2. The Eq. (19) can be solved by discretizing L by a set of node points. The functions G_{ij}^m and H_{ij}^m in Eq. (19) can be obtained from the displacement Green's functions G_{ij} given in the Appendix. All Green's functions appear in terms of semi-infinite integrals with complex-valued oscillatory integrands. Rajapakse and Wang (1993) discussed the numerical evaluation of the Green's functions. In the present study, numerical quadrature is applied to evaluate the Green's functions following the details given by Rajapakse and Wang (1993). The application of numerical quadrature to Eq. (19) together with the treatment of singularities is extensively discussed by Banerjee (1994). For cylindrical foundations, integration of Green's functions over the tributary areas can be carried out analytically for constant elements except for diagonal terms. The application of numerical quadrature to Eq. (19) results in the following matrix relationship between displacements and tractions at node points on L.

$$\frac{1}{2}\boldsymbol{I}\boldsymbol{u}^m + \overline{\boldsymbol{H}}^m \boldsymbol{u}^m = \overline{\boldsymbol{G}}^m \boldsymbol{T}^m \tag{21}$$

where $\boldsymbol{I}$ is a unit matrix; $\boldsymbol{u}^m$ and $\boldsymbol{T}^m$ denote the mth harmonic of nodal displacement and traction vectors respectively.

For a vertically loaded foundation, the matrices $\overline{\boldsymbol{G}}^0$ and $\overline{\boldsymbol{H}}^0$ corresponding to Green's functions integrated over nodal tributary areas can be expressed as

$$\overline{\boldsymbol{H}}^0_{2M\times 2M} = \begin{pmatrix} \overline{H}^0_{rr}(\boldsymbol{x}_i, \overline{\boldsymbol{x}}_j) & \overline{H}^0_{zr}(\boldsymbol{x}_i, \overline{\boldsymbol{x}}_j) \\ \overline{H}^0_{rz}(\boldsymbol{x}_i, \overline{\boldsymbol{x}}_j) & \overline{H}^0_{zz}(\boldsymbol{x}_i, \overline{\boldsymbol{x}}_j) \end{pmatrix} \tag{22}$$

$$\overline{\boldsymbol{G}}^0_{2M\times 2M} = \begin{pmatrix} \overline{G}^0_{rr}(\boldsymbol{x}_i, \overline{\boldsymbol{x}}_j) & \overline{G}^0_{zr}(\boldsymbol{x}_i, \overline{\boldsymbol{x}}_j) \\ \overline{G}^0_{rz}(\boldsymbol{x}_i, \overline{\boldsymbol{x}}_j) & \overline{G}^0_{zz}(\boldsymbol{x}_i, \overline{\boldsymbol{x}}_j) \end{pmatrix} \tag{23}$$

Table 1 Convergence of impedances with number of node points (h/a=1.0, a_0=1.0, ν=0.25)

M	K_V	K_H	K_M
10	(7.52, 10.61)	(9.28, 11.01)	(11.37, 5.16)
13	(7.34, 10.45)	(9.31, 11.01)	(11.37, 5.15)
15	(7.29, 10.40)	(9.29, 10.99)	(11.26, 5.16)
17	(7.25, 10.38)	(9.26, 10.96)	(11.25, 5.16)
20	(7.24, 10.37)	(9.24, 10.94)	(11.25, 5.16)
Ref. [3]	(7.57, 10.79)	(9.30, 11.13)	(11.31, 5.32)

Table 2 Comparison of impedances at different frequencies (h/a=1.0, M=15, ν=0.25)

a_0		0.25	1.50	2.00
K_V	Present	(8.44,2.68)	(7.11,16.07)	(6.76,22.01)
	Ref.[3]	(8.25,2.73)	(6.94,16.57)	(6.44,22.70)
K_H	Present	(9.73,2.90)	(8.82,16.49)	(8.39,22.18)
	Ref.[3]	(9.57,2.96)	(8.90,16.57)	(8.49,22.70)
K_M	Present	(13.58,0.58)	(10.57,8.84)	(9.98,12.46)
	Ref.[3]	(13.44,0.75)	(10.60,9.03)	(10.11,12.76)

For a laterally loaded foundation the matrices $\overline{\boldsymbol{G}}$ and $\overline{\boldsymbol{H}}$ can be expressed as

$$\overline{\boldsymbol{H}}^{l}_{3M\times 3M}=\begin{pmatrix} \overline{H}^{l}_{rr}(x_i,\overline{x}_j) & \overline{H}^{l}_{\theta r}(x_i,\overline{x}_j) & \overline{H}^{l}_{zr}(x_i,\overline{x}_j)\\ \overline{H}^{l}_{r\theta}(x_i,\overline{x}_j) & \overline{H}^{l}_{\theta\theta}(x_i,\overline{x}_j) & \overline{H}^{l}_{z\theta}(x_i,\overline{x}_j)\\ \overline{H}^{l}_{rz}(x_i,\overline{x}_j) & \overline{H}^{l}_{\theta z}(x_i,\overline{x}_j) & \overline{H}^{l}_{zz}(x_i,\overline{x}_j) \end{pmatrix} \tag{24}$$

$$\overline{\boldsymbol{G}}^{l}_{3M\times 3M}=\begin{pmatrix} \overline{G}^{l}_{rr}(x_i,\overline{x}_j) & \overline{G}^{l}_{\theta r}(x_i,\overline{x}_j) & \overline{G}^{l}_{zr}(x_i,\overline{x}_j)\\ \overline{G}^{l}_{r\theta}(x_i,\overline{x}_j) & \overline{G}^{l}_{\theta\theta}(x_i,\overline{x}_j) & \overline{G}^{l}_{z\theta}(x_i,\overline{x}_j)\\ \overline{G}^{l}_{rz}(x_i,\overline{x}_j) & \overline{G}^{l}_{\theta z}(x_i,\overline{x}_j) & \overline{G}^{l}_{zz}(x_i,\overline{x}_j) \end{pmatrix} \tag{25}$$

A solution for $\boldsymbol{T}^m$ can be obtained from Eq. (21)

$$\boldsymbol{T}^m=(\overline{\boldsymbol{G}}^m)^{-1}(\tfrac{1}{2}\boldsymbol{I}+\overline{\boldsymbol{H}}^m)\boldsymbol{u}^m \quad m=0,\ 1 \tag{26}$$

The vector $\boldsymbol{u}^m$ in the above equation can be expressed in terms of Δ_V by using Eqs. (10) and (11) for vertically loaded foundations, and in terms of Δ_H and ϕ_y for laterally (including moment) loaded foundations. Therefore, the vector $\boldsymbol{T}^m$ can be expressed in terms of Δ_V or Δ_H and ϕ_y. The integrals in Eqs. (15)-(17) can be reduced to integrals over L and subsequent application of numerical quadrature with Eq. (26) results in the solution for impedances defined by the Eq. (18).

IV. NUMERICAL SOLUTIONS AND DISCUSSION

The numerical stability and accuracy of the boundary element solutions are studied by varying the number of node points (M) on the generating curve S of a foundation. A cylindrical foundation with length-radius ratio h/a=1.0 in an isotropic soil is initially considered. Table 1 shows numerical solutions for impedances K_V, K_H and K_M for different values of M. These results correspond to normalised frequency $a_0[a_0=\omega a(\rho/c_{44})^{1/2}]$=1.0. In the case of cylindrical foundations, the impedances computed in this study are defined with respect to the center of the foundation base [i.e. point A has coordinates (0, 0, h)] Table 1 also shows the impedances reported by Apsel and Luco (1987) for the same problem using an indirect boundary element approach. The results obtained in the present study are numerically very stable and are in close agreement with those reported by Apsel and Luco (1987). Table 2 presents a comparison of impedances of a cylindrical foundation with h/a=1.0 at a_0=0.25, 0.75, 1.5, 2.0 with Apsel and Luco (1987). A comparison of present solutions and those given by Luco and Wong (1986) for a rigid hemispherical foundation is given in Table 3. In the case of hemispherical foundations, the impedances are defined with respect to the coordinate origin (i.e, point A is at O) to facilitate comparisons with Luco and Wong (1986). The numerical results presented in Tables 1 to 3 clearly confirms the accuracy and numerical

Table 3 Comparison of impedances of a hemispherical foundation (M=20, ν=0.25)

a_0		0.01	1.00	2.00
K_V	Present	(7.19,0.00)	(6.93,7.57)	(6.60,15.11)
	Ref.[17]	(7.19,0.00)	(7.01,7.64)	(6.62,15.54)
K_H	Present	(7.96,0.00)	(7.98,7.73)	(7.72,15.33)
	Ref.[17]	(7.95,0.00)	(8.03,7.97)	(7.75,15.55)
K_M	Present	(10.36,0.00)	(9.08,3.01)	(8.34, 7.42)
	Ref.[17]	(10.34,0.00)	(9.09,3.18)	(8.35, 7.59)
K_{HM}	Present	(4.06,0.00)	(4.18,3.23)	(4.12, 6.44)
	Ref.[17]	(3.98,0.00)	(4.16,3.32)	(4.09, 6.49)

stability of the present boundary element solutions.

Numerical solutions for impedances of rigid cylindrical and hemispherical foundations are presented in Figs. 3-7. The soils considered in this study are silty clay, beryl rock, clay and an isotropic soil. The relevant material constants are given in Table 4 where normalised constant $\overline{c}_{ij}=c_{ij}/c_{44}$ is used. The frequency range $0.0<a_0\leq 2.0$ is considered in the numerical study since most forced vibrations of machine foundations are within this range (Gazetas, 1983).

It is noted from Figs. 3-6 that the real part of vertical impedance, *ie.* $Re(K_V)$, of cylindrical foundations decreases smoothly as the frequency a_0 increases for h/a=0.25, 0.5 and 1.0. A minor increase is initially noted for very small frequencies. However, for h/a=2.0, $Re(K_V)$ decreases in the range $0\leq a_0\leq 0.8$ and thereafter increases slowly with increasing frequency. The general trend of variation of $Re(K_V)$ with a_0 is similar for all four materials although the magnitude of $Re(K_V)$ depends considerably on the type of soil. The influence of material anisotropy on $Re(K_V)$ is also evident. The largest $Re(K_V)$ is found for a foundation in beryl rock followed by foundations in clay, isotropic soil and silty clay. The imaginary part of K_V shows a linear variation with a_0 for 0. $0\leq a_0\leq 2.0$. The influence of material anisotropy on $Im(K_V)$ is generally negligible and become smaller with increasing a_0. The order of magnitude of K_V can be related to the order of magnitude of $\overline{c}_{33}$ in Table 4. This implies that the influence of material anisotropy on the vertical impedance is mainly governed by the normalised material constant $\overline{c}_{33}$ representing the elastic moduli of the soil in the vertical direction.

The real part of horizontal impedance K_H of cylindrical foundations is nearly independent of a_0 for $h/a\leq 0.5$. However, for $h/a\geq 1.0$, $Re(K_H)$ gradually decreases with increasing a_0. The imaginary part of K_H shows a near linear variation with a_0 similar to the case of $Im(K_V)$. The influence of material anisotropy is more significant on the real part of the horizontal impedance and relatively smaller on the imaginary part of K_H. The largest $Re(K_H)$ corresponds to a foundation in clay followed by foundations in beryl rock, isotropic soil and silty clay. The influence of soil anisotropy increases slightly with increasing h/a and a_0. A comparison of the order of magnitudes of K_H and normalised material constants in Table 4 indicates that the influence of material anisotropy on K_H is mainly reflected by the value of $\overline{c}_{11}$.

The real part of rocking impedance K_M decreases gradually with the frequency for cylindrical foundations. The variation of $Re(K_M)$ with frequency is similar for the four soils. Soil anisotropy has a strong influence on $Re(K_M)$ for shorter foundations ($h/a\leq 0.5$) that is similar to the case of $Re(K_V)$. For $h/a\geq 1.0$, the $Re(K_M)$ of a foundation in clay is slightly greater than a foundation in beryl rock. Therefore it appears that the influence of material anisotropy on $Re(K_M)$ cannot be related to a single value of $\overline{c}_{ij}$ in Table 4. A linear variation with the frequency is noted for $Im(K_M)$ for $a_0>0.6$. $Im(K_M)$ of shorter foundations ($h/a\leq 1.0$) show less dependence on the soil type. Radiation damping in clay is found to be the highest for rocking mode of vibrations followed by foundations in beryl rock, isotropic soil and silty clay.

Figs. 3-6 indicate that for shorter foundations ($h/a\leq 0.5$), the real part of the coupled impedance (K_{HM}) initially increases with the frequency for $0\leq a_0\leq 1.0$ and thereafter decreases. However for h/a=1.0, 2.0, the real part of coupled impedance shows a gradual increase with a_0. $Re(K_{HM})$ also shows a strong dependence on the degree of material anisotropy similar to the real parts of other impedance components. The highest influence of material anisotropy on $Re(K_{HM})$ is noted for a foundation in silty clay and followed by foundations in isotropic soil, beryl rock and clay. A similar influence of soil anisotropy is noted on the profiles of $Im(K_{HM})$. The imaginary part of the coupled impedance shows the highest influence of soil anisotropy when compared

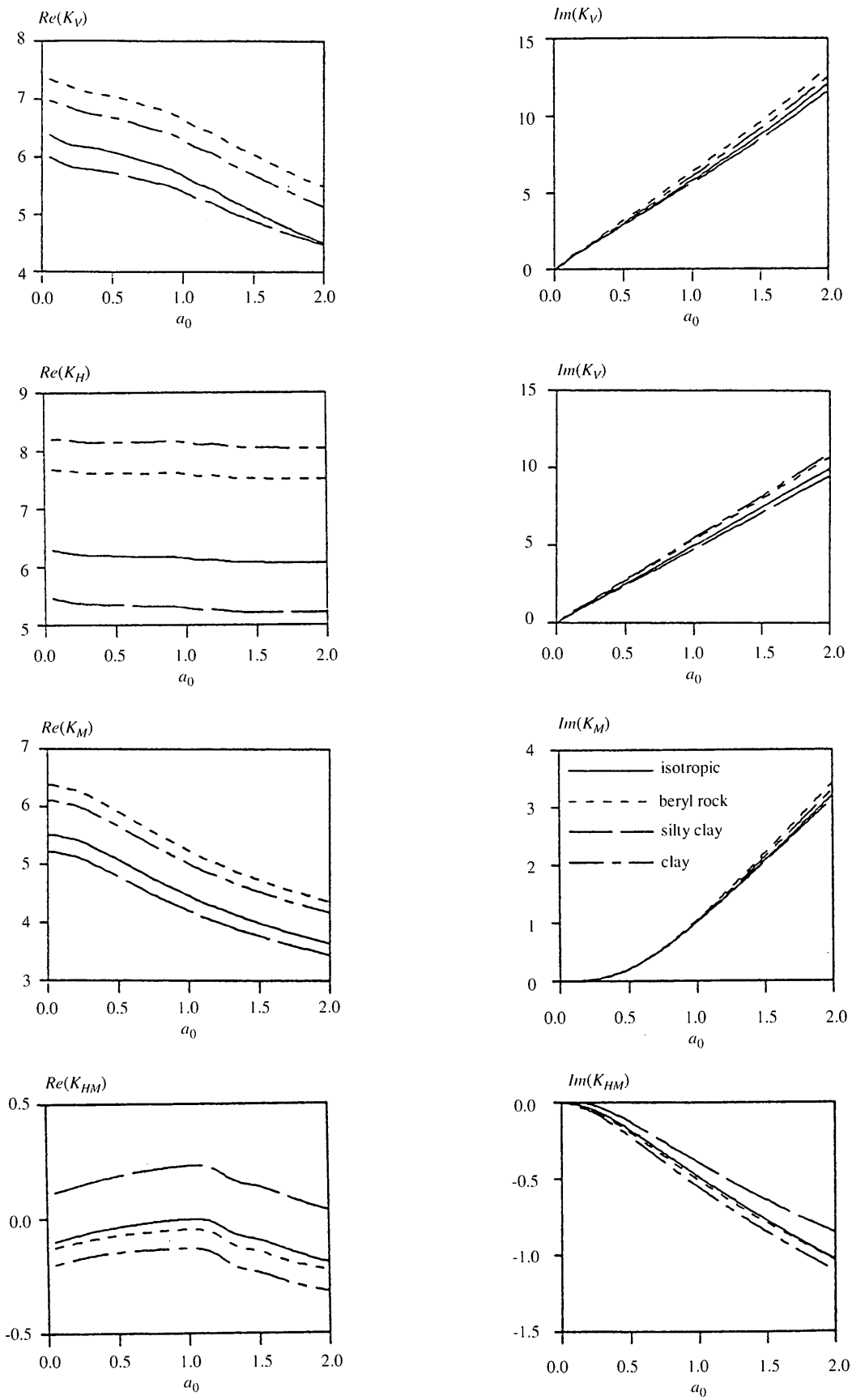

Fig. 3 Impedances of a rigid cylindrical foundation (h/a=0.25, M=10)

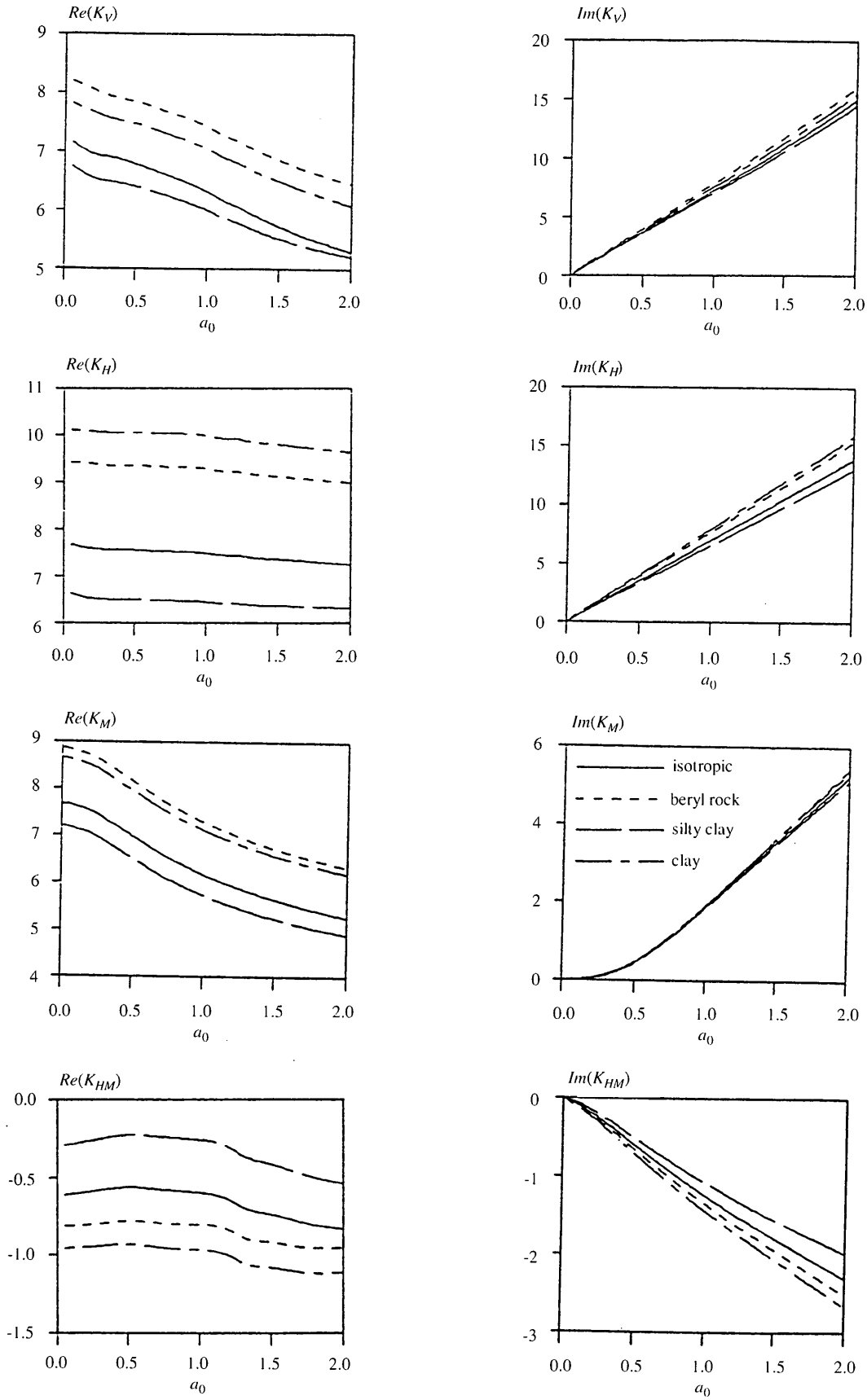

Fig. 4 Impedances of a rigid cylindrical foundation (h/a=0.50, M=12)

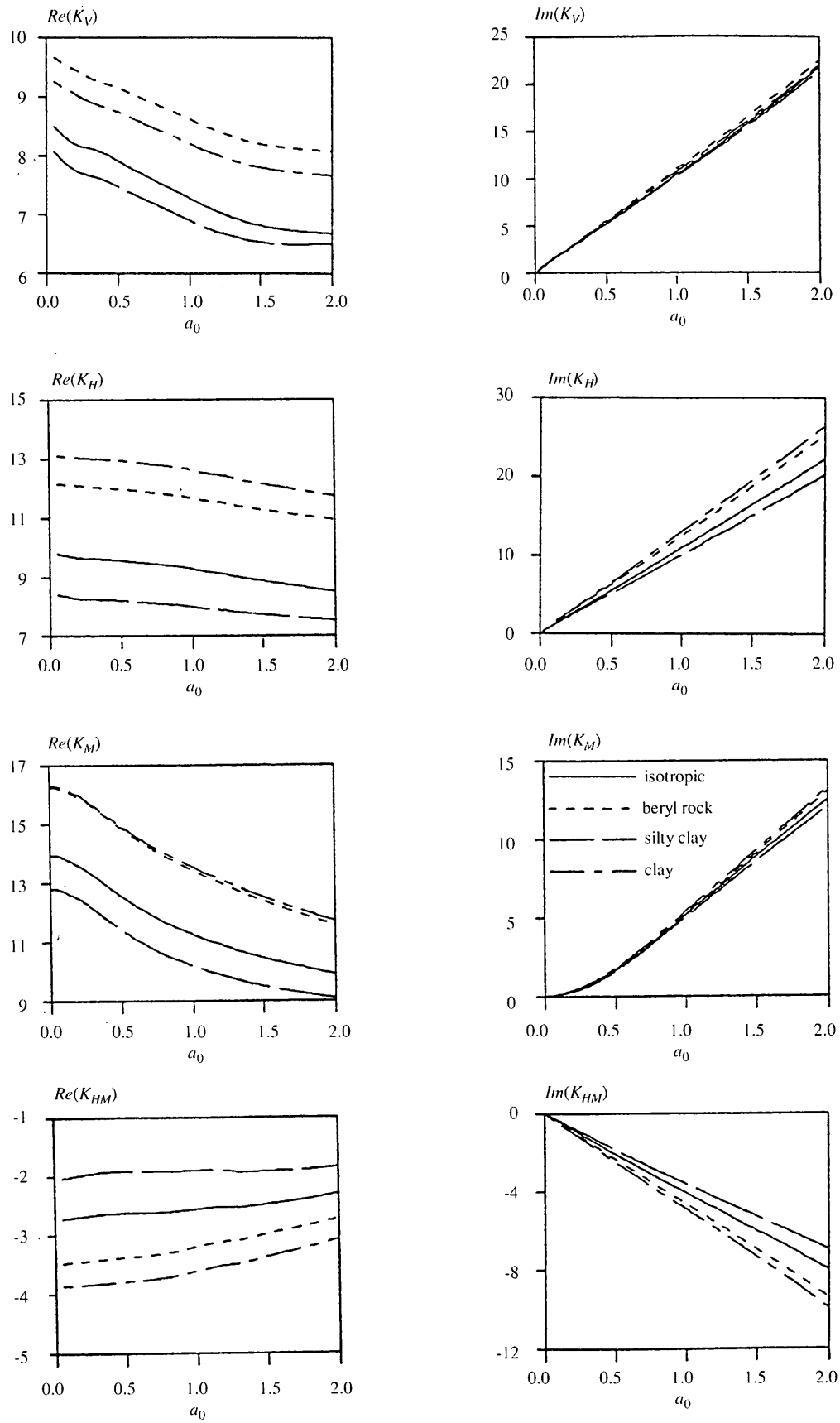

Fig. 5 Impedances of a rigid cylindrical foundation (h/a=1.0, M=15)

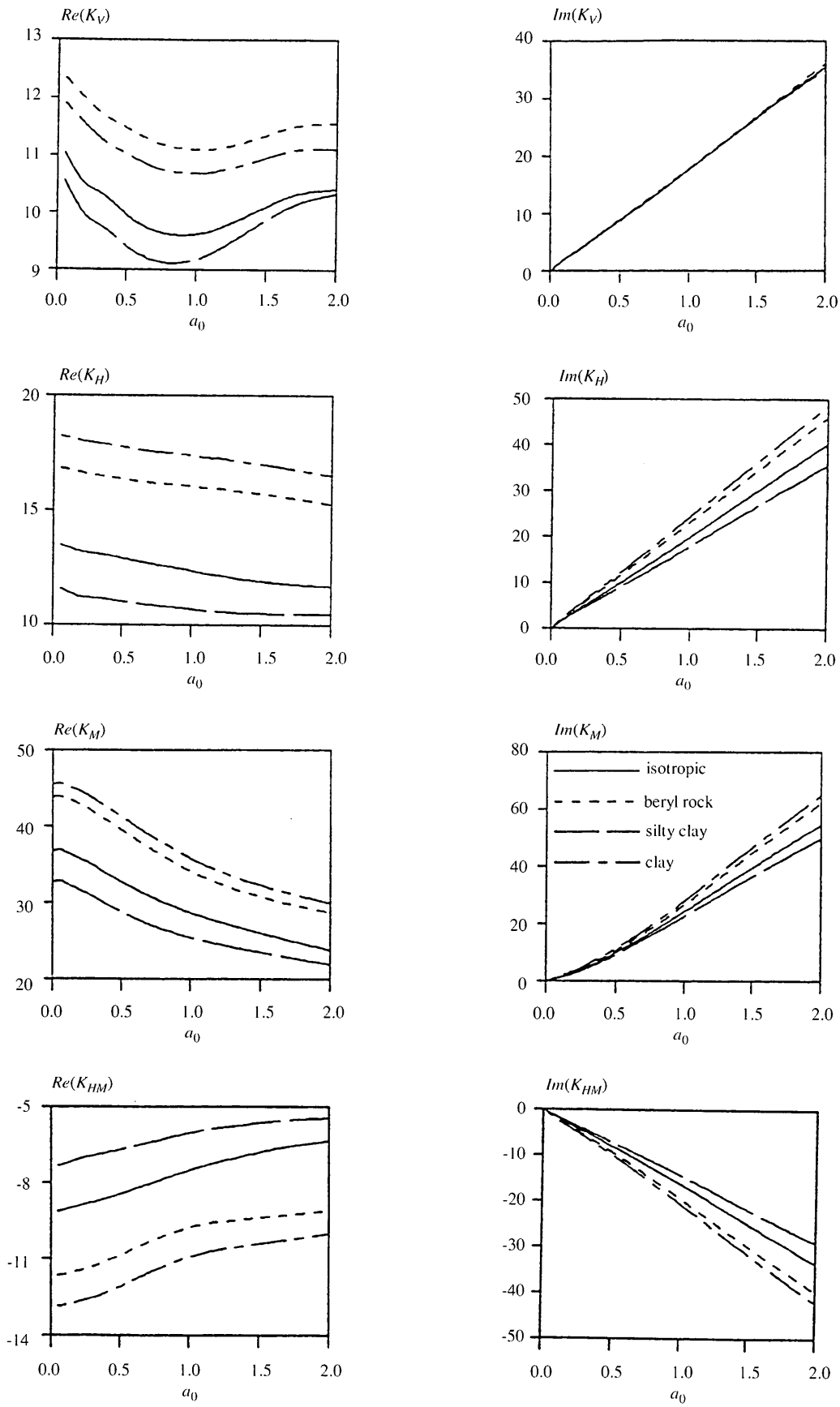

Fig. 6 Impedances of a rigid cylindrical foundation (h/a=2.0, M=17)

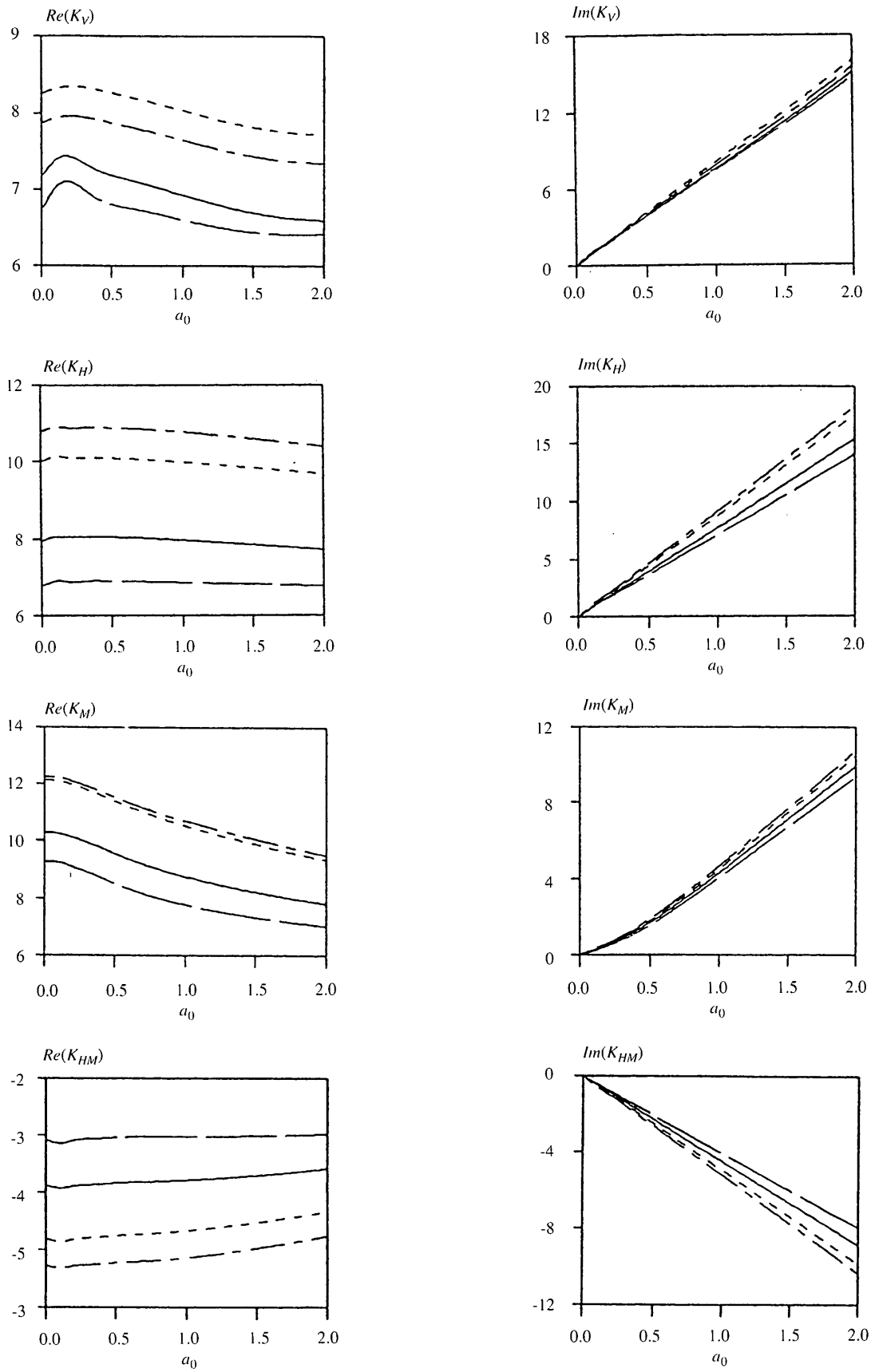

Fig. 7 Impedances of rigid hemispherical foundation (M=20)

Table 4 Normalized material constants

Material	c_{11}	c_{12}	c_{33}	c_{13}	$c_{44}(\times 10^4$ N/mm^2)
Iotropic	3.00	1.00	3.00	1.00	1.00
Beryl rock	4.13	1.47	3.62	1.01	1.00
Silty clay	2.11	0.43	2.58	0.47	2.70
Clay	4.70	1.70	3.30	1.20	0.01

to imaginary parts of other impedances. $Im(K_{HM})$ decreases linearly with a_0. Comparison of the order of magnitudes of K_{HM} and the normalised material constants in Table 4 indicates that the influence of material anisotropy on K_{HM} is similar to that seen previously for K_H and can be related to $\overline{c}_{11}$.

Figure 7 show the solutions for impedances of a massless hemispherical foundation of radius 'a'. A comparison of K_V, K_H, K_M and K_{HM} profiles indicates that the variation of impedances with frequency is almost identical to that of cylindrical foundations with h/a=0.5 and 1.0. Note that the coupled impedance show different magnitudes since the point A is defined at the coordinate origin in the case of hemispherical foundations. The magnitude of diagonal impedances are generally smaller than the corresponding values for a cylindrical foundation with h/a=1.0 and higher than those corresponding to h/a= 0.5. The dependence of impedances on soil anisotropy also show trends identical to that noted previously for cylindrical foundations. Comparison of solutions in Figs. 3-7 indicate that impedances depend significantly on the foundation geometry. An increase in the depth/radius ratio generally results in increases in both real and imaginary parts of impedances.

V. CONCLUSIONS

The boundary element method based on Green's functions of a transversely isotropic medium is successfully applied to study the dynamic response of rigid axisymmetric foundations. Numerical solutions for vertical, horizontal, rocking and coupled impedances of foundations in four soils are presented. The impedances significantly depend on the frequency of excitation, degree of anisotropy of soil and the geometry of foundation. The variation of real parts of impedances with frequency is non-oscillatory whereas the imaginary parts show near linear variation with frequency. The magnitudes of real and imaginary parts of impedances increase with increasing depth of embedment. The influence of soil anisotropy on the vertical impedances is related to the normalised elastic modulus $\overline{c}_{33}$. In the case of horizontal and coupled impedances, the influence of soil anisotropy is governed mainly by $\overline{c}_{11}$. The degree of material anisotropy has a relatively smaller influence on the imaginary parts (radiation damping) of impedances when compared to the real parts. The dynamic response of a hemispherical foundation is quite similar to that of cylindrical foundation with h/a=1.0. The present methodology can be extended to study foundations with other axisymmetric geometries and situations involving loss of contact with the surrounding soils.

ACKNOWLEDGEMENT

The work presented here was supported by grant A-6507 from the Natural Sciences and Engineering Research Council of Canada.

REFERENCES

1. Apsel, R.J., 1979, "Dynamic Green's Functions for Layered Media and Applications to Boundary-value Problems," *Ph.D. Thesis*, University of California, USA.
2. Apsel, R.J., and Luco, J.E., 1976, "Torsional Response of a Rigid Embedded Foundation," *J. Engng. Mechanics*, ASCE, Vol. 102, pp. 957-970.
3. Apsel, R.J., and Luco, J.E., 1987, "Impedance Functions for Foundations Embedded in a Layered Medium: An Integral Equation Approach," *Earthquake Engng. Struct. Dyn.*, Vol. 15, pp. 213-221.
4. Banerjee, P.K., 1994, *The boundary element methods in engineering*, McGraw-Hill, England.
5. Baranov, V.A., 1967, "On the Calculation of Excited Vibrations of an Embedded Foundation" (in Russian), *Voprosy Dynamiki: Prochnocti*, 14, Polytechnical Institute of Riga, pp. 195-209.
6. Day, S.M., 1977, "Finite Element Analysis of Seismic Scattering Problems," *Ph.D. Thesis*, University of California, USA.
7. Dominguez, J., 1978, "Dynamic Stiffness of Rectangular Foundations," *Report* R78-20, Dept. of Civil Engineering, MIT, USA.
8. Freedman, J.M., and Keer, L.M., 1972, "Vibratory Motion of a Body on an Orthotropic Half Plane," *J. Applied Mechanics*, ASME, Vol. 39, pp. 1033-1040.
9. Gazetas, G., 1981, "Strip Foundations on Cross-anisotropic Soil Layer Subjected to Static and Dynamic Loading," *Geotechnique*, Vol. 31, pp. 161-179.
10. Gazetas, G., 1983, "Analysis of Machine Foundation Vibrations: State of the Art," *Soil Dyna. Earthquake Engng.*, Vol. 2, pp. 2-42.
11. Gibson, R.E., 1974, "The Analytical Method in Soil Mechanics," *Geotechnique*, Vol. 24, pp.

115-140.
12. Kausel, E., and Roesset, J.M., 1975, "Dynamic Stiffness of Circular Foundations," *J. Engng. Mechanics*, ASCE, Vol. 101, pp. 771-785.
13. Kirkner, D.J., 1979, "Steady-state Response of a Circular Foundation on a Transversely Isotropic Half-space," *Ph.D. Thesis*, Case Western Reserve University, USA.
14. Kuhlemeyer, R.L., 1969, "Vertical Vibrations of Footings Embedded in Layered Media," *Ph.D. Thesis*, University of California, USA.
15. Lekhnitskii, S.G., 1963, *Theory of anisotropic elastic bodies*, Holden-Day Publishing Co., California.
16. Luco, J.E., 1976, "Torsional Response of Structures for SH Waves: the Case of Hemispherical Foundations," *Bull. Seism. Soc. Am.*, Vol. 66, pp. 109-124.
17. Luco, J.E., and Wong, H.L., 1986, "Dynamic Response of a Hemispherical Foundation Embedded in a Viscoelastic Half Space," *J. Engng. Mechanics*, Vol. 112, pp. 1363-1374.
18. Novak, M., and Beredugo, Y.O., 1972, "Vertical Vibration of Embedded Footings," *J. Soil Mech. Found.*, ASCE, Vol. 98, pp. 1291-1310.
19. Payton, R.G., 1983, *Elastic wave propagation in transversely isotropic media*,' Martinus Nijhoff, The Netherlands .
20. Rajapakse, R.K.N.D., and Wang, Y., 1993, "Green's Functions for a Transversely Isotropic Elastic Half Space," *J. Engng. Mechanics*, ASCE, Vol. 119, pp. 1724-1746.
21. Rizzo, F.J., Shippy, D.J., and Rezayat, M., 1985, "Boundary Integral Equation Analysis for a Class of Earth-Structure Interaction Problems," *Report*, Dept. of Engineering Mechanics, University of Kentucky, USA.
22. Wang, Y., and Rajapakse, R.K.N.D., 1991, "Dynamics of Rigid Strip Foundations Embedded in Orthotropic Elastic Soils," *Earthquake Engng. Struc. Dyn.*, Vol. 20, pp. 927-947.
23. Wass, G., 1972, "Linear Two-dimensional Analysis of Soil Dynamics Problems in Semi-infinite Layered Media," *Ph.D. Thesis*, University of California, USA.

APPENDIX I

The displacement Green's functions corresponding to the ring loading shown in Fig. 2 can be expressed as

$$G_{ij}(r, \theta, z; s, z') = \frac{\delta^2}{c_{44}} \int_0^\infty \hat{G}_{ij}^m \zeta d\zeta \quad i, j = r, \theta, z \tag{A1}$$

where m=0 for loading shown in Figs. 2(a) and 2(b), and m=1 for loading shown in Figs. 2(c)-2(e), and

$$\hat{G}_{rz}^m = \cos m\theta \frac{p_1}{RV}(a_1\rho_2\bar{e}_1 + Ia_1\rho_2\bar{e}_2 + a_2\rho_1\bar{e}_3 - Ia_2\rho_1\bar{e}_4 - a_1\rho_1\bar{e}_5 - a_2\rho_2\bar{e}_6) \tag{A2}$$

$$\hat{G}_{\theta z}^m = -\sin m\theta \frac{p_1}{RV}(a_4\rho_2\bar{e}_1 - Ia_4\rho_2\bar{e}_2 + a_5\rho_1\bar{e}_3 + Ia_5\rho_1\bar{e}_4 - a_4\rho_1\bar{e}_5 - a_5\rho_2\bar{e}_6) \tag{A3}$$

$$\hat{G}_{zz}^m = \cos m\theta \frac{p_1}{RV}(a_7\rho_2\bar{e}_1 - a_7\rho_2\bar{e}_2 + a_8\rho_1\bar{e}_3 + a_8\rho_1\bar{e}_4 - a_7\rho_1\bar{e}_5 - a_8\rho_2\bar{e}_6) \tag{A4}$$

$$\hat{G}_{r\theta}^m = \cos m\theta[\frac{(p_2+p_3)}{RS}(a_1\xi_2\bar{e}_1 - a_1\xi_2\bar{e}_2 + a_2\xi_1\bar{e}_3 + a_2\xi_1\bar{e}_4 - a_1\xi_1\bar{e}_5 - a_2\xi_2\bar{e}_6) - \frac{(p_2-p_3)}{\xi_3}a_3(\bar{e}_7 + \bar{e}_8)] \tag{A5}$$

$$\hat{G}_{\theta\theta}^m = -\sin m\theta[\frac{(p_2+p_3)}{RS}(a_4\xi_2\bar{e}_1 - a_4\xi_2\bar{e}_2 + a_5\xi_1\bar{e}_3 + a_5\xi_1\bar{e}_4 - a_4\xi_1\bar{e}_5 - a_5\xi_2\bar{e}_6) - \frac{(p_2-p_3)}{\xi_3}a_6(\bar{e}_7 + \bar{e}_8)] \tag{A6}$$

$$\hat{G}_{z\theta}^m = \cos m\theta \frac{(p_2+p_3)}{RS}(a_7\xi_2\bar{e}_1 - Ia_7\xi_2\bar{e}_2 + a_8\xi_1\bar{e}_3 + Ia_8\xi_1\bar{e}_4 - a_7\xi_1\bar{e}_5 - a_8\xi_2\bar{e}_6) \tag{A7}$$

$$\hat{G}_{rr}^m = -\cos m\theta[\frac{(p_2-p_3)}{RS}(a_1\xi_2\bar{e}_1 - a_1\xi_2\bar{e}_2 + a_2\xi_1\bar{e}_3 + a_2\xi_1\bar{e}_4 - a_1\xi_1\bar{e}_5 - a_2\xi_2\bar{e}_6) + \frac{(p_2+p_3)}{\xi_3}a_3(\bar{e}_7 + \bar{e}_8)] \tag{A8}$$

$$\hat{G}_{\theta r}^m = \sin m\theta[\frac{(p_2-p_3)}{RS}(a_4\xi_2\bar{e}_1 - a_4\xi_2\bar{e}_2 + a_5\xi_1\bar{e}_3 + a_5\xi_1\bar{e}_4 - a_4\xi_1\bar{e}_5 - a_5\xi_2\bar{e}_6) + \frac{(p_2+p_3)}{\xi_3}a_6(\bar{e}_7 + \bar{e}_8)] \tag{A9}$$

$$\hat{G}_{zr}^m = -\cos m\theta \frac{(p_2-p_3)}{RS}(a_7\xi_2\bar{e}_1 - Ia_7\xi_2\bar{e}_2 + a_8\xi_1\bar{e}_3 + Ia_8\xi_1\bar{e}_4 - a_7\xi_1\bar{e}_5 - a_8\xi_2\bar{e}_6) \tag{A10}$$

In eqns (A2)-(A10),

$$R=\frac{K(\xi_1-\xi_2)}{\kappa\delta^2\zeta^2} \tag{A11}$$

$$V=\alpha(\xi_1^2-\xi_2^2)(\zeta^2+1)/\kappa\zeta^2,\quad S=\alpha\delta^2\xi_1\xi_2(\xi_1^2-\xi_2^2)/\kappa\zeta^2 \tag{A12}$$

$$p_1=\frac{p_0 sJ_m(\delta\zeta s)}{2},\quad p_2=\frac{p_0 sJ_{m-1}(\delta\zeta s)}{4},\quad p_3=\frac{p_0 sJ_{m+1}(\delta\zeta s)}{4} \tag{A13}$$

$$f_1=\xi_1(1+\rho_1)[\alpha\xi_1^2-(\kappa-1)\zeta^2\rho_1] \tag{A14}$$

$$f_2=\xi_2(1+\rho_2)[\alpha\xi_2^2-(\kappa-1)\zeta^2\rho_2] \tag{A15}$$

$$f_3=\xi_2(1+\rho_2)[\alpha\xi_1^2-(\kappa-1)\delta^2\rho_1]+\xi_1(1+\rho_1)[\alpha\xi_1^2-(\kappa-1)\delta^2\rho_2] \tag{A16}$$

$$\overline{e}_1=f_3e^{-\delta\xi_1(z'+z)};\quad \overline{e}_2=Re^{-\delta\xi_1|z'-z|};\quad \overline{e}_3=f_3e^{-\delta\xi_2(z'+z)} \tag{A17}$$

$$\overline{e}_4=Re^{-\delta\xi_2|z'-z|};\quad \overline{e}_5=2f_1e^{-\delta(\xi_1 z+\xi_2 z')};\quad \overline{e}_6=2f_2e^{-\delta(\xi_1 z'+\xi_2 z)} \tag{A18}$$

$$\overline{e}_7=e^{-\xi_3(z'+z)};\quad \overline{e}_8=e^{-\xi_3|z'-z|} \tag{A19}$$

$$\frac{a_7}{\delta\xi_1}=\frac{a_8}{\delta\xi_2}=J_m(\delta\zeta r) \tag{A20}$$

$$a_3=\frac{a_4}{\rho_1}=\frac{a_5}{\rho_2}=\frac{\delta\zeta[J_{m-1}(\delta\zeta r)+J_{m+1}(\delta\zeta r)]}{2} \tag{A21}$$

$$a_6=\frac{a_1}{\rho_1}=\frac{a_2}{\rho_2}=\frac{\delta\zeta[J_{m-1}(\delta\zeta r)-J_{m+1}(\delta\zeta r)]}{2} \tag{A22}$$

$$\rho_1=\frac{\alpha\xi_1^2-\zeta^2+1}{\kappa\zeta^2},\quad \rho_2=\frac{\alpha\xi_2^2-\zeta^2+1}{\kappa\zeta^2} \tag{A23}$$

$$\xi_1=\frac{(\gamma\zeta^2-1-\alpha+\sqrt{\Phi})^{\frac{1}{2}}}{\sqrt{2\alpha}};\quad \xi_2=\frac{(\gamma\zeta^2-1-\alpha-\sqrt{\Phi})^{\frac{1}{2}}}{\sqrt{2\alpha}} \tag{A24}$$

$$\Phi=(\gamma\zeta^2-1-\alpha)^2-4\alpha(\beta\zeta^4-\beta\zeta^2-\zeta^2+1) \tag{A25}$$

$$\xi_3=\pm\sqrt{\varsigma\zeta^2-1} \tag{A26}$$

and $\zeta=\lambda/\delta$ and λ is the Hankel transform parameter; $\delta=\omega(\rho/c_{44})^{1/2}$; α, β, κ, γ and ς are nondimensional material parameters defined as

$$\alpha=\frac{c_{33}}{c_{44}},\quad \beta=\frac{c_{11}}{c_{44}},\quad \kappa=\frac{(c_{13}+c_{44})}{c_{44}},$$

$$\gamma=1+\alpha\beta-\kappa^2,\quad \varsigma=\frac{(c_{11}-c_{12})}{2c_{44}} \tag{A27}$$

Discussions of this paper may appear in the discussion section of a future issue. All discussions should be submitted to the Editor-in-Chief.

Manuscript Received: Dec. 21, 1999
Revision Received: Jan. 10, 2000
and Accepted: Feb. 05, 2000

嵌入橫向等向性土壤之剛性基礎動力邊界元素分析

Yaoping Wang and Nimal Rajapakse

加拿大 Manitoba 大學土木及地質學系

摘 要

本文探討在質量可忽略之圓柱與半球形剛性基礎嵌入橫向等向彈性土壤之動力反應。假設基礎的對稱軸與土壤材料對稱軸平行，基礎承受沿著水平方向與垂直方向的簡諧力與簡諧彎矩。我們以邊界元素法分析此問題。其中邊界積分方程式中的核函數爲受到圓環載重之半無窮域橫向等向性土壤之彈動力格林函數。文中採用解析的格林函數。本文以基礎嵌入橫向等向性土壤的阻抗解與近年來研究得到的等向土壤結果做比較。幾個選擇算例說明了土壤異向性、激發頻率及基礎幾何形狀對阻抗的影響。

關鍵詞：異向性，邊界元素法，動力，基礎。